Radio Wave Diffusion Indoors and Throughput Scaling with Cell Density

Dmitry Chizhik, *Senior Member, IEEE*, Jonathan Ling, *Member, IEEE*, Reinaldo A. Valenzuela, *Fellow, IEEE*

***Abstract*—Diffusion theory is found to provide a simple yet accurate expression for the average received radio power loss indoors in non-line-of-sight propagation. Effective specific absorption is the sole parameter. Agreement with extensive indoor power measurements is found at all ranges. Use of the standard power-law to describe the data is found to lead to power exponents that vary from near 2 at short ranges to around 11 at 100 m. Extending the diffusion model to account for variation in scatterer density provides a stochastic mechanism explaining the log-normal nature of observed average power variations, usually termed "shadow fading". The standard deviation of power variation is found to increase with range (as $r^{1/2}$ at short ranges), in agreement with measurements and unlike accepted models. Exponential absorption in diffusion is determined to have a large impact on the signal-to-interference-and noise behavior, materially affecting conclusions on the value of increasing cell density as a method of increasing wireless network capacity.**

***Index Terms*—Diffusion, small cells, indoor environment, propagation loss.**

I. Introduction

INCREASING the capacity of wireless systems is often achieved through increasing density of cells, with intercell interference a major performance impairment. Distribution of radio wave power with range determines the signal-to-interference and noise ratio (SINR), a critical performance-defining parameter. Among the widely used methods of estimating radio signal characteristics, ray tracing is considered the most accurate [1]-[5], with building layout and materials a necessary input. The results are site-specific and, for the purposes of general performance assessment, more generic models are often desired. A generic model should have "sufficient" accuracy, simplicity and be non-proprietary. Addressing this need, empirical models of path loss, based on fit to measurements, as well as theoretical models based on transport theory and its diffusion approximation have been reported in the literature.

Widely used empirical models of path loss as a function of range *r* in wireless systems represent it as a power law:

$$P_{\mathrm{L}} = -10\log_{10}\left(\frac{a}{(r/r_0)^n}\right) = P_{\mathrm{L}_0} + 10n\log_{10}(r/r_0), (\mathrm{dB}) \quad (1)$$

parametrized by the "distance-exponent" *n* and "intercept" $P_{\mathrm{L}_0} \equiv -10\log_{10}(a)$, defined as path loss in dB at reference range r_0. The law has been reported by Hata [7] to be representative of path loss measured by Okumura, et. al. [6] outdoors, and, in many cases, indoors. While deviations from (1) are usually described empirically as normally distributed shadow fading (in dB), in [8][9] it was reported that making the exponent *n* also a random variable provides a good description of indoor data. Path loss laws of the form (1) have been incorporated into standard models [10]. It has been also found to be well justified theoretically [11][12] in outdoor, macrocellular environments. Refinements of (1) also exist that represent path loss (in dB) dependence on $\log_{10} r$ as a broken line with two slopes, separated by a breakpoint, with the goal of accounting for the expected near-free-space r^{-2} behavior at short range, followed by the far steeper r^{-11} loss at larger ranges indoors [13]. Measurements of indoor path loss in non-line of sight scenarios are reported here as well that show that at large ranges in such environments the slope-intercept model is not a good depiction of the path loss behavior and, in fact, its parameters would change substantially depending on ranges of interest. A path loss law dependent on range *r*, wavelength λ and specific attenuation rate α as

$$P_{\mathrm{G}} = \left(\frac{\lambda}{4\pi r}\right)^2 e^{-\alpha r} \quad (2)$$

was found to be an effective description of propagation loss in [15] and [16], although Medbo [15] has also reported good agreement with (1), excluding long range data (>40 m) and segregating locations into morphology types, such as line-of-sight (LOS) and non-line-of-sight (NLOS). Laws of the form (2) are a continuous medium form of the Keenan-Motley [17] law, which consists of free space spreading loss and an "excess loss" (in dB) to every wall traversed on the direct path from receiver to transmitter.

Taking a more fundamental approach, Ullmo and Baranger [18] have formulated and solved numerically the statistical Boltzmann equation and analytically its diffusion approximation. Effects modeled statistically were scattering by walls and "loss' attributed to scattering outside the building. Both 2D and 3D diffusion were considered, but 2D was decided upon for comparison to data, i.e. the photons are allowed to spread in a plane as opposed to all three spatial dimensions. The results were found to agree well with measurements outside the region of 15 m and poorly at closer ranges. Janaswamy [19] reported successful use of the 2D transport theory in modeling "excess loss" indoors at 60 GHz. Franceschetti, et. al. [19] have made elegant use of homogeneous photon diffusion in 3D to find good agreement with outdoor urban path loss measurements for low antennas at ranges up to 300 m.

Current work addresses propagation modeling in cluttered, non-line-of-sight (NLOS) circumstances of interest in large scale, multicell indoor networks. Preliminary discussion of various indoor propagation mechanisms in Section II of this

Manuscript received September 27, 2011; revised February 20 and March 30, 2012; accepted April 9, 2012. The associate editor coordinating the review of this paper and approving it for publication was C. Yang.

The authors are with Bell Laboratories, Alcatel-Lucent, Holmdel, NJ 07733 (e-mail: Dmitry.Chizhik@alcatel-lucent.com).

Digital Object Identifier 10.1109/TWC.2012.062012.111779

work is used to explain the choice of the model of the environment and its idealization. In Section III we find that the radiative transfer theory, well developed in physics, also in the diffusion approximation, leads to a simple expression for signal strength, valid for 3D diffusion, that agrees well with measurements at all ranges of an extensive indoor data set, as well as with published measurement results. In Section IV we show that statistical inhomogeneity in effective absorption over space leads to log-normally distributed "shadow fading", whose standard deviation increases with range, in agreement with measurements, and unlike standard models that hold such standard deviation constant. In Section V we show through numerical simulation that using the resulting model as opposed to the power law leads to significantly different conclusions on the SINR distribution and the relative value of a dense grid of indoor cells. Novel contributions include the finding that standard 3D diffusion is an accurate representation of NLOS indoor path loss measurements, the experimental finding that the variance of shadow fading increases with range, theoretical derivation of range-dependent shadow fading variance, and the finding that the exponential absorption in indoor diffusion leads to a degradation in system capacity gain with increasing cell density, attributed to a rise in interference with shrinking cell size.

II. The Indoor Environment and its Idealization

A. Single floor as a lossy parallel plate waveguide

Different floors of commercial buildings are typically separated by reinforced concrete, also often with a sheet of corrugated steel. Inter-floor attenuation has been reported to be high, with the signal path thought to be through various "openings" (like stairways, gaps around pipes, etc.), as well as through diffraction/scattering outside the building [21]. Here we limit ourselves to single floor propagation, confined between two effectively impenetrable floor slabs. The space between the floor slabs ($\sim$ 3 m) is many times the wavelength of interest ($\sim$ 0.15 m). In the absence of clutter, the environment is idealized as an overmoded parallel plate waveguide, with a lossy boundary, i.e. the concrete floor (and ceiling, if not covered by steel). Propagation from a point source in such an environment may be viewed as a superposition of guided (and evanescent) modes everywhere, but it is useful to separate it into 2 regions: short range, where the dominant mechanism is the spreading loss associated with the field "filling" the space, similarly to what happens in free space, and longer range, where the field has "filled" the (vertical) extent of the guide and each mode propagates with its own characteristic phase speed and attenuation, as well as cylindrical spreading $1/r$. Attenuation is very significant for higher order modes, leaving only lower order modes as effective energy-bearers [22]. Fine structure associated with modal phase interference is present in both regimes. Average power received by a canonical small antenna would then decay with range r as $1/r^2$ at short ranges, followed by $1/r$ propagation (cylindrical spreading in a parallel plate guide). Exponential losses due to absorption become prominent at very long ranges. We observe that power laws $1/r^n$ provide the most dramatic relative decrease in power at short ranges, while the exponential loss e^{-ar} obviously leads to power decay that is linear (in dB) with range. It may be shown that the average received power in an overmoded parallel-plate guide of typical dimension (3 m high, supporting about 20 modes at 2 GHz) with lossy walls begins to significantly deviate from spherical spreading at ranges beyond 100 m, due to transition to cylindrical spreading ($1/r$). Exponential absorption loss is present throughout, as discussed in section III, and the signals are found to be greatly attenuated at this transition range. For typical wireless settings (e.g. 100 mW transmit power and 10 MHz bandwidth at 2 GHz center frequency) the signal levels at the transition range are below thermal noise. It is therefore decided that, for estimating average power at ranges of interest, the single-floor waveguide is large enough to be better approximated as a 3D medium rather than a 2D one. This captures proper spreading loss at ranges below 100 m and slightly overestimates loss at longer ranges, where signals are generally weak. Since the eventual goal is to study interference-limited systems, weak signals from distant sources play a relatively small part.

B. Effect of scatterers

Of particular interest here are large buildings where multiple cells are likely to be deployed. The environment contains many scatterers, such as walls and furniture. Scattering from such objects is thought to be lossless, primarily re-distributing the energy, not removing it. Metallic objects act as strong scatterers, with minimal penetration into the object. The primary loss mechanism at radio frequencies is taken to be due to scattering from objects containing moisture, such as concrete [23]. Of course the energy "absorbed" is not really lost but is rather converted into heat and re-radiated across a wide band in the form of black-body radiation.

In summary, for the mathematical treatment and comparison to data, the indoor environment will be approximated as a statistically homogeneous 3D medium, filled with partially absorbing scatterers. In Section IV the model is extended to include spatial variability in effective absorption as a mechanism causing "shadow fading".

III. Average Path Loss Based on Homogeneous Diffusion

The approach considered here is through the use of transport theory in the diffuse scattering approximation [24], whose results are briefly summarized in the beginning of this section for completeness. The fundamental quantity is the specific intensity, $I(\mathbf{r}, \hat{s})$ representing power density in W/m^2/steradian at point $\mathbf{r}$ in direction $\hat{s}$, consisting of the coherent intensity and diffuse intensity:

$$I(\mathbf{r}, \hat{s}) = I_{\mathrm{c}}(\mathbf{r}, \hat{s}) + I_{\mathrm{d}}(\mathbf{r}, \hat{s}) \tag{3}$$

Coherent (sometimes called reduced) intensity may be determined through modeling of all the known scattering phenomena. In homogeneous scattering media with scatterer density ρ and total scattering cross-section σ_t , the coherent intensity obeys the differential equation with path length parameter s:

$$\frac{dI_{\mathrm{c}}(\mathbf{r}, \hat{s})}{ds} = -\rho\sigma_{\mathrm{t}} I_{\mathrm{c}}(\mathbf{r}, \hat{s}) \tag{4}$$

whose solution is

$$I_{\mathrm{c}}(\mathbf{r}, \hat{s}) = I_{\mathrm{c}}(0, \hat{s}) e^{-\rho\sigma_{\mathrm{t}} s} \tag{5}$$

In this section we are interested in modeling propagation in cluttered environments where the total cross-section σ_t is large, making coherent intensity (5) small at ranges of interest. The specific intensity (3) is then dominated by the diffuse term. We further represent scattering as being nearly isotropic (not generally valid for each individual scatterer but becoming valid after propagation through several rooms). The average intensity, defined as the average over the solid angle ω:

$$U_0(\mathbf{r}) = \frac{1}{4\pi}\int_0^{4\pi} I_{\rm d}(\mathbf{r},\hat{s})d\omega \tag{6}$$

satisfies the diffusion equation [24]:

$$\nabla^2 U_0 - \kappa_{\rm d}^2 U_0 = -\frac{3}{4\pi}\rho\sigma_{\rm tr}P_{\rm T}\delta(\mathbf{r}), \tag{7}$$

where point source term on the right is of power P_T and $\sigma_{\rm tr}$ is the transport cross-section [24], which for isotropic scattering approaches the total scattering cross-section, $\sigma_{\rm tr} \approx \sigma_{\rm t}$. The quantity $\kappa_{\rm d}^2$ is related to scatterer densityρ and absorption cross-section $\sigma_{\rm a}$through $\kappa_{\rm d}^2 = 3\rho\sigma_{\rm a}\rho\sigma_{\rm tr} \approx 3\rho^2\sigma_{\rm a}\sigma_{\rm t}$. Here $\kappa_{\rm d}^2$ will be treated as an empirical quantity as the effective scatterer density and cross-sections of office furniture are known only to an order of magnitude and further rigor in this aspect would run counter to the phenomenological treatment adapted here. Solution to (7) takes the form:

$$U_0 = \frac{e^{-\kappa_{\rm d}r}}{4\pi r}\left[\frac{3}{4\pi}\rho\sigma_{\rm tr}P_{\rm T}\right]. \tag{8}$$

From which the flux density (W/m^2) follows (equation (9-13) in [24])as

$$\mathbf{F}_{\rm d} = -\frac{4\pi}{3\rho\sigma_{tr}}\nabla U_0 = \left[\frac{\kappa_{\rm d}}{4\pi r} + \frac{1}{4\pi r^2}\right]e^{-\kappa_{\rm d}r}P_{\rm T}\hat{r}. \tag{9}$$

Path gain $P_{\rm G} = P_{\rm R}/P_{\rm T}$ for a unity gain antenna of effective area $\frac{\lambda^2}{4\pi}$is then

$$P_{\rm G} = \frac{\lambda^2}{4\pi}\left[\frac{\kappa_{\rm d}}{4\pi r} + \frac{1}{4\pi r^2}\right]e^{-\kappa_{\rm d}r}. \tag{10}$$

In the absence of absorption, $\kappa_{\rm d} = 0$, (10) reduces to the standard Friis formula for free space path gain.

Extensive narrowband path loss measurements have been conducted in the 1990's on the second floor of a 3-story office building, whose layout, with color-coded measurements is illustrated in Figure 1. The floors of the building were separated by slabs of re-enforced concrete, with each floor 3 m high. Exterior walls were concrete with ordinary glass windows, while interior walls were sheetrock and ordinary glass partitions. The rooms were furnished with common office furniture. The measurements, centered at 2 GHz, included several transmitter locations, with receive antennas at a multitude of locations, with maximum range of 57 m. Transmitter and receiver antennas were placed 1.8 meters above the floor. Each reported path loss measurement is actually a local average of received powers, with receive antenna translated horizontally over a region of several wavelengths, so as to remove the effect of short scale fading. Of interest in this work are the non-LOS locations where the conditions for diffusion are expected to be satisfied. Prediction (10) of path loss ($-10\log_{10}P_{\rm G}$) as a function of range may be compared against measurements in Figure 2, over the available transmitter-receiver separation of

Fig. 1. Office building, obstructed data locations for one sample data set. Transmitter location for this data set is marked by an arrow

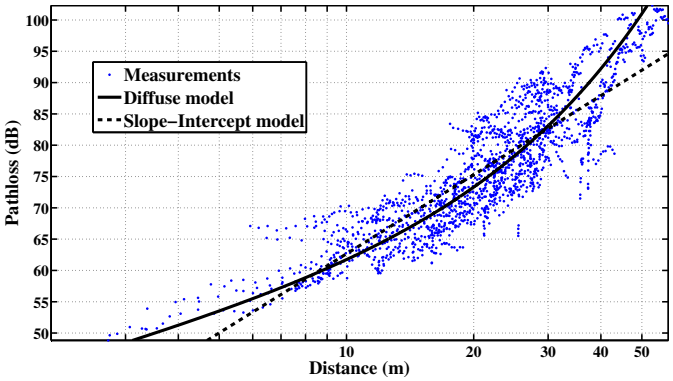

Fig. 2. Comparison of measured path loss to diffusion and power-law models. Best fit parameters for diffusion: κ_d = 0.77 dB/m and for power-law: n=4.3, 1-m path loss = 20 dB

TABLE I
RMS DIFFERENCE BETWEEN MEASURED PATH LOSS AND MODELS

***Rms* "error" for diffuse model, κ_d= 0.77 dB/m (0.18 nepers/m)**	***Rms* "error" for power-law model (2 parameters, n=4.3, 1-m path loss = 20 dB)**
4.8 dB	4.9 dB

3 m – 57 m. The rms error of the two models is tabulated in Table 1. It may be observed that the exponential model offers a slightly better fit (by 0.1 dB rms) while using only a single adjustable parameter κ_d.

While the accuracy advantage may appear modest over this range, the two models do begin to diverge strongly at larger ranges. The values of the exponent n in the best fit power-law model is found to depend strongly on the maximum range of the data set, varying from 2 at short ranges to over 4 at intermediate ranges (57 m here). Enormous losses ($\sim$ 140 dB) have been measured indoors at ranges of 100 m [13][15]. Devasirvatham, et. al. [14] and Medbo, et. al. [15] have found that an empirical path gain model $P_{\rm G} = \lambda^2/(4\pi r)^2 e^{-\alpha r}$, similar in form to (10), was representative of measured path loss at ranges up to 100 m. It is found here that using the absorption value κ_d= 0.77 dB/m (0.18 nepers/m), provides best fit to data in Figure 2, and gives a reasonably accurate prediction for data reported by Medbo [15] as well. Since it is

accurate, one can examine the consequences of fitting a power law (1) in an environment where (10) holds, even at ranges exceeding the maximum range of measurements in Figure 2. To do so, a synthetic path loss "data" set was generated numerically by dropping receivers uniformly in a circle of radius 100 m, centered around a transmitter. Path loss for each receiver location was evaluated using (10), multiplied by a log-normally distributed shadow fading factor, whose standard deviation is derived in the following section. A power-law fit of form (1) to this "data" produces an exponent n=10.5. The high value of the exponent n is broadly consistent with n=11.5 reported for measurements in [13], where it was attributed to diffraction effects modeled through ray tracing. Diffusion modeling, as done here, succeeds in modeling these effects. This is not in contradiction to ray tracing but rather a statement that diffusion is emergent and is an effective simple model. We therefore conclude that no single value of the distance exponent in the power-law model (1) describes the path loss dependence on range, with n varying from 2 at short ranges to about 4 at intermediate ranges ($\sim$ 57 m) to over 10 at longer ranges ($\sim$ 100 m). On the other hand, the diffusion model (10) remains representative across all ranges with a single parameter κ_d (=0.77 dB/m in the data set in Figures 1 and 2).

IV. Shadowing Variation

An obvious observation coming from comparison of the measured and predicted values of locally averaged signal in Figure 2 is that the data shows considerable deviation from path loss predicted using (10). As the measured data is actually a local average of received power over an area of about 0.5 m in diameter (i.e. $>> \lambda/2$), it is thought short scale spatial variation coming from coherent interference of arrivals (aka Rayleigh fading) has been largely removed [26]. The data-model difference in Figure 2 is traditionally modeled empirically as a random variable following a normal distribution in dB, or, equivalently, a log-normal distribution in actual power. It is often termed as "shadow fading", particularly outdoors. It is of interest to find a theoretical basis for such variation and explore some of the consequences. Diffusion equation (7) is now generalized to include spatially varying scattering cross-section:

$$\nabla^2 U_{\rm d} - \kappa_{\rm d}^2(\mathbf{r})\, U_{\rm d} = -\frac{3}{4\pi}\rho\sigma_{\rm tr} P_{\rm T}\delta(\mathbf{r}). \tag{11}$$

Spatially variable scattering manifests itself in characteristic effective absorption $\kappa_{\rm d}(\mathbf{r})$ consisting of constant and spatially fluctuating parts:

$$\kappa_{\rm d}(\mathbf{r}) = \bar{\kappa}_{\rm d} + \kappa_{\rm f}(\mathbf{r}) \tag{12}$$

The spatial variability in indoor radio propagation is taken to represent variation in wall and furniture density and composition. The effective absorption $\kappa_{\rm d}(\mathbf{r})$ is defined at a point $\mathbf{r}$ in terms of the local density and average cross-section of scatterers [24], as summarized after (7). These quantities are, in turn, local averages, defined within a certain region encompassing many scatterers. Since scatterer separation is on the order of 1 m, this region is the size of one or more rooms. Such averaging tends to result in smoothly varying quantities. For example, the presence of a narrow office hallway manifests itself as a general reduction in specific absorption $\kappa_{\rm d}(\mathbf{r})$, not as a sharply defined region with no scatterers. The fluctuating part of the characteristic absorption is defined as having zero mean, $\langle \kappa_{\rm f}(\mathbf{r})\rangle = 0$, and "small" rms amplitude, $\left\langle |\kappa_{\rm f}(\mathbf{r})|^2 \right\rangle^{1/2} << \bar{\kappa}_{\rm d}$, leading to

$$\kappa_{\rm d}^2(\mathbf{r}) \approx \bar{\kappa}_{\rm d}^2 + 2\bar{\kappa}_{\rm d}\kappa_{\rm f}(\mathbf{r}). \tag{13}$$

Weak fluctuation in $\kappa_{\rm d}(\mathbf{r})$is justified when considering variations in scatterer density between offices as well as between offices and narrow hallways, whose width is on the order of separation between office furniture. It is not satisfied when considering environments where either one or both ends of the link are in or near the same hallway, where hallway guiding effects introduce structure incompatible with the diffuse scattering assumptions. Likewise, presence of a large atrium is also incompatible with diffuse scattering. In these environments, structure must be included and other theories, such as that of waveguides and full transport theory, without the diffusion approximation, is called for [24]. It is now observed that the spatially inhomogeneous diffusion equation (11) differs from the Helmholtz equation for single frequency coherent wave propagation only in the sign of the second term on the left, suggesting that corresponding approximate methods of solving (11) may be brought to bear. For slowly varying $\kappa_{\rm f}(\mathbf{r})$, $|\nabla\kappa_{\rm f}(\mathbf{r})| << (\bar{\kappa}_{\rm d} + \kappa_{\rm f}(\mathbf{r}))^2$, Rytov [24] or Method of Smooth Perturbations [25] may be used to find approximate solution to (11). Briefly, the method presents the solution as a product of the reference solution U_0 and $U_1 \equiv e^{\psi_1}$

$$U_{\rm d} = U_0 U_1 = U_0 e^{\psi_1}, \tag{14}$$

with reference solution U_0 for homogeneous diffusion (7) given by (8). Substitution of (14) and (13) into (11) allows a formulation of a series solution. The first term ψ_{10} in the series is used in weak fluctuation theory, resulting in:

$$\psi_{10} = \frac{-2\bar{\kappa}_{\rm d}}{U_0}\int_{V'} dV' G(\mathbf{r}-\mathbf{r}')\ \ \kappa_{\rm f}(\mathbf{r}')\ U_0(\mathbf{r}') \tag{15}$$

Weak fluctuation theory is valid [25] in the limit $\left\langle |\nabla_\perp \psi_{10}|^2 \right\rangle << 2\bar{\kappa}_{\rm d}\left\langle |\kappa_{\rm f}|^2 \right\rangle^{1/2}$, verified to hold for the ψ_{10} solution obtained below. The Greens function is the solution to the normalized equation of the form (7):

$$G(\mathbf{r}-\mathbf{r}') = \frac{e^{-\bar{\kappa}_{\rm d}|\mathbf{r}-\mathbf{r}'|}}{4\pi|\mathbf{r}-\mathbf{r}'|} \approx \frac{e^{-\bar{\kappa}_{\rm d}(x-x') - \bar{\kappa}_{\rm d}\frac{|\boldsymbol{\rho}-\boldsymbol{\rho}'|^2}{2(x-x')}}}{4\pi(x-x')} \tag{16}$$

The approximation in (16) is the paraxial approximation, with x-axis taken as the line containing the transmitter and receiver, and $\boldsymbol{\rho}$ is the 2D coordinate in the plane orthogonal to the x-axis, not to be confused with scatterer density ρ. The perturbation in specific absorption $\kappa_{\rm f}(r)$ is presumed to be known only statistically, and is taken to be a zero-mean process with known spatial covariance. Following Ishimaru [24], (15) may be evaluated first for a plane wave illumination, $U_0 = e^{-\bar{\kappa}_{\rm d}x}$, from which the expression for the case of the spherical wave illumination (8) can be derived. For a plane wave, the log-power fluctuation (15) becomes

$$\psi_{10} = -2\bar{\kappa}_{\rm d}\int_0^x dx' \iint_{-\infty-\infty}^{\infty\ \ \infty} d\boldsymbol{\rho}' \frac{e^{-\bar{\kappa}_{\rm d}\frac{|\boldsymbol{\rho}-\boldsymbol{\rho}'|^2}{2(x-x')}}}{4\pi(x-x')}\ \kappa_{\rm f}(x',\boldsymbol{\rho}') \tag{17}$$

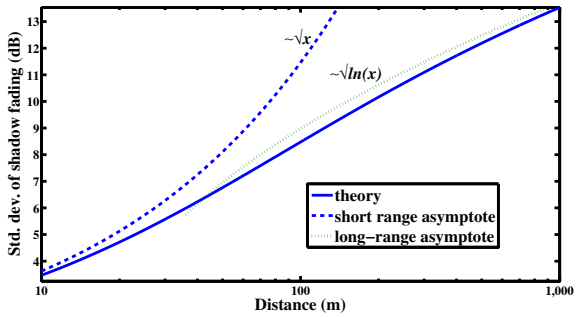

Fig. 3. Standard deviation of shadow fading (dB), $\left\langle |\psi_{10}|^2 \right\rangle^{1/2} 10\log_{10} e$, as a function of range using (A-11), with short and long range asymptotes, following (18)

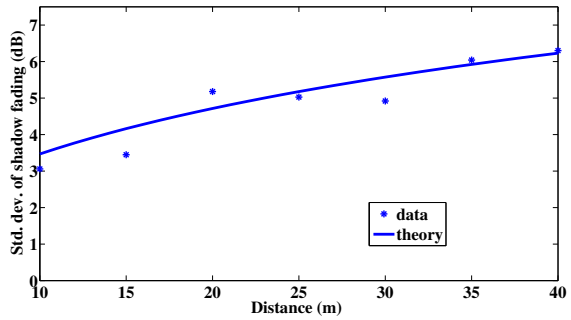

Fig. 4. Observed and theoretical range dependence of the shadow fading standard deviation $\langle |\psi_{10}|^2 \rangle^{1/2} 10\log_{10}$ dB. Parameters used for theoretical curve: $\left\langle |\kappa_{\rm f}|^2 \right\rangle^{1/2} = 0.25\bar{\kappa}_{\rm d}, l$= 20m, $\bar{\kappa}_{\rm d}$=0.18 nepers/m.

where the axial and transverse integrals are stated explicitly. It may be observed that the approximation (17) for log-power fluctuation is a weighted continuous sum (i.e. integral) of random variation of the effective absorption $\kappa_{\rm f}(r)$. Once the receiver-transmitter range is many times the coherence scale of $\kappa_{\rm f}(r)$, (17) may be regarded as a sum of independent random variables. As range increases, by Central Limit Theorem, log-power approaches a normal distribution, and, the variations in intensity U_d in (14) are, thus, log-normal. Similar observations have already been established when using the Rytov approximation in the solution of the Helmholtz equation [25]. Here it is seen as arising in the case of the diffusion equation as well. The log-normal nature of the shadow fading variation may therefore be attributed to spatially varying effective absorption. The extent of log-power variation, quantified by the standard deviation of (17), is derived in the Appendix using spectral methods. The resulting standard deviation is found to depend on range, with short and long range asymptotes given by:

$$\langle |\psi_{10}|^2 \rangle^{1/2} \approx \begin{cases} \sqrt{\pi^{1/2}\langle |\kappa_{\rm f}^2| \rangle l x}, & \bar{\kappa}_{\rm d} l^2 >> x \\ \sqrt{\frac{\pi^{1/2}}{2}\langle |\kappa_{\rm f}|^2 \rangle l^3 \bar{\kappa}_{\rm d} \ln \left| \frac{4x}{\bar{\kappa}_{\rm d} l^2} \right|}, & \bar{\kappa}_{\rm d} l^2 << x. \end{cases} \tag{18}$$

where l is the characteristic coherence scale of the fluctuating part κ_f of the specific absorption. Note that the standard deviation of "shadow fading" expressed in dB is $\left\langle |\psi_{10}|^2 \right\rangle^{1/2} 10\log_{10} e$. At short ranges the standard deviation is seen to scale with range as $\sqrt{x}$, which is the same dependence as would arise when modeling the absorption as a random walk in one dimension. For long ranges, the standard deviation scales with x as a slower function $\sqrt{\ln x}$. This may be attributed to path diversity in 3D: variations are somewhat less dramatic with range if the diffusion allows the photons to arrive at the receiver while going around obstacles rather than trying to penetrate the obstacles. The range dependence of the two asymptotes (18) is illustrated with the standard deviation following from variance (A-11) in Figure 3. Notably, an empirical model of randomly distributed exponent n in (1) also leads a distance-dependent "shadow fading", but of somewhat different form [9].

Empirical standard deviation of the indoor data described in Section III was computed as a function of range for data subsets within 2 m range "windows" centered around a nominal range. The resulting standard deviations, along with predictions using (A-11) are shown in Figure 4 as a function of nominal range. The empirical standard deviation is seen to double as the range increases from 10 m to 40 m. Parameters found to provide a good fit to the observed variation are : $\left\langle |\kappa_{\rm f}|^2 \right\rangle^{1/2} = 0.25\,\bar{\kappa}_{\rm d}$, l = 20 m, $\bar{\kappa}_{\rm d}$ = 0.18 nepers/m. It is concluded that the observed values of shadow fading standard deviation increase with range substantially and consistent with diffusion theory. Normalized measured "shadow fading" may be computed from data by removing average distance-dependent loss (10) and normalizing the resulting "shadowing" by $\left\langle |\psi_{10}|^2 \right\rangle^{1/2} 10\log_{10} e$, using (A.11). The cumulative distribution of the result is compared against a standard normal distribution in Figure 5. A similarly close match was reported in [9].

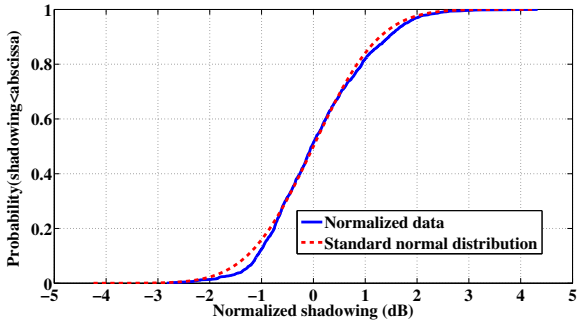

Fig. 5. Cumulative distribution of measured "shadow fading", normalized by $\left\langle |\psi_{10}|^2 \right\rangle^{1/2} 10\log_{10} e$, and compared against standard distribution $N(0,1)$. Actual data has standard deviation of "shadow fading" varying with range (Figure 4) and is 4.8 dB on average.

V. Impact on Throughput Scaling with Cell Density

Above it was argued that propagation loss indoors is better described by (10) as opposed to the outdoor formula (1). We are interested in finding the consequences of this change in propagation law on performance of a multicell wireless system. To assess this through a numerical simulation, the wireless system is idealized as a regular hexagonal grid of cells, each of area $A_{\rm c}$, covering a large region of total area A.

A base station of transmit power P_{T} is placed at the center of each cell, with every base station using the same bandwidth B (aka universal re-use). Since all cells are assumed to be statistically identical, the overall system capacity is thus A/A_{c} times the capacity achieved within each cell. A large number of mobiles are uniformly distributed over a plane, with each mobile associating with the strongest base station. Signals from all the other base stations constitute interference and no attempt is made here to manage it. Signal strengths from the desired and interfering base stations depend on the random location of the mobile. The performance metric chosen here is the distribution of rates experienced by mobiles in different locations, and scaled to the entire network. Adapting Shannon's classical formula, network spectral efficiency depends on signal–to-interference+noise-ratio (SINR) Γas:

$$C = \frac{A}{A_{\mathrm{c}}} \log_2 (1+\Gamma), \quad (bps/Hz) \tag{19}$$

where the factor of A/A_{c} is the number of cells in the large network and it is assumed that multiple users within a cell are orthogonally multiplexed. Insight into system behavior may be gained by defining area spectral efficiency R_a, (bps/Hz/km^2):

$$R_{\mathrm{a}} = \frac{C}{A} = \frac{1}{A_{\mathrm{c}}} \log_2 (1+\Gamma) \tag{20}$$

The SINR ratio Γ for the power law (1) is:

$$\Gamma = \frac{P_{\mathrm{T}} \frac{a}{(r_d/r_0)^n} \varsigma_d}{\sum\limits_{\substack{k=1,\\ k\neq d}}^{K} P_{\mathrm{T}} \frac{a}{(r_k/r_0)^n} \varsigma_k + N_0} \tag{21}$$

where ranges to r_d and r_k are ranges to desired and interfering bases, respectively, ς_d and ς_k corresponding shadow fading realizations (conventionally *iid* log-normal variates) and N_0 is the noise power spectral density. Systems striving for high capacity are often interference limited. Dropping noise power N_0 in the denominator in consideration of this limit, it may be observed that Γ in (21) is no longer dependent on the reference range r_0. For path loss (1), area spectral efficiency (20) is seen to simply increase linearly with cell density ($\sim 1/A_c$), with every cell experiencing size-independent SINR (21). This is termed "cell-splitting gain". In such an environment, to double capacity, cell density needs to be doubled.

Consistent with indoor path gain described by (10) as opposed to (1), it is of interest to determine resulting SINR scaling with indoor cell size. SINR Γ is again a random variable depending both on ranges to serving and interfering bases as well as shadow fading realizations. Distributions of the simulated SINR, obtained by uniform sampling of the network area are shown in Figure 6 for a hexagonal network of cells with cell separations ranging from 6 m to 50 m. As cell size decreases, the SINR decreases, in contrast to behavior of (21), arising from models of type (1). This may be attributed to the exponential decay in path gain (10), which masks distant interferers more effectively than closer ones. The path gain behavior with range may be qualitatively separated into 2 zones: the near zone where algebraic factor $\left[\frac{\kappa_d}{4\pi r} + \frac{1}{4\pi r^2}\right]$ in (10) dominates and the far zone, where $e^{-\kappa_d r}$ is prominent. As cell density increases (i.e. cell size decreases), greater number of interferers are included within the near zone, leading to a

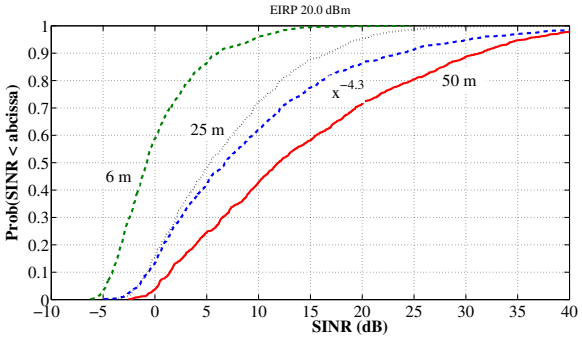

Fig. 6. SINR distributions for different cell separations in the diffuse scattering (indoor) environment, exhibiting SINR degradation as cells shrink. The scale-invariant SINR for a path gain power law $x^{-4.3}$ is also shown for comparison.

degradation in SINR, with corresponding decrease in per user (Shannon) spectral efficiency, $\log_2(1+\Gamma)$. We can deduce from Figure 6 that as cell separation decreases from 50 m to 25 m, observed decrease in median SINR from 14 dB to 7 dB leads to a reduction in median per user spectral efficiency from 4.7 bps/Hz to 2.6 bps/Hz, or a factor of 0.55. At the same time, halving of the cell radius quadruples cell density. System throughput may then be expected to increase by a factor of 0.55 x 4 = 2.2. Thus, quadrupling the cell density gives a little more than doubling of system capacity. Overall trends in area spectral efficiency are illustrated in Figure 7. It may be observed that capacity in a diffuse medium at 50 m cell separation is higher than that predicted using a power law path loss. This is attributed to more effective "masking" of interferers in a diffuse medium at this range. Decreasing the cell separation from 50 m to 6 m corresponds to increasing the cell density by a factor of about 69($\sim 50^2/6^2$), precisely the factor by which the area spectral efficiency scales when path gain follows the power law (here $x^{-4.3}$). In contrast, such an increase in cell density when using the diffusion model for path gain leads to an increase in spectral efficiency by a factor of "only" 12. Thus, using the conventional power law model leads to an overprediction of cell-splitting gain by almost 6$\times$ ($\sim$ 69/12). Comparable observations were made in [27], where under a path loss law (2), similar to (10), it was shown that capacity scales as $\sim \sqrt{\text{cell density}}$. Primary reason for this scaling is the presence of exponential absorption in path gain law (10), with shadow fading playing a minor role. We conclude that the diffusion model leads to a degradation in SINR indoors as cell density increases, partially offsetting cell splitting gains.

VI. Conclusions

Measured average radio propagation loss dependence on range in non-line-of-sight (NLOS) is found to be well described by a simple expression (10) derived by modeling propagation as diffusion in a 3D medium, with a single parameter (specific absorption) dependent on the environment. Measured standard deviation of the received log-power, i.e. "shadow fading", increases with range substantially. Consideration of statistical variation of the scatterer density over space is found to lead to a prediction of the power variation, both

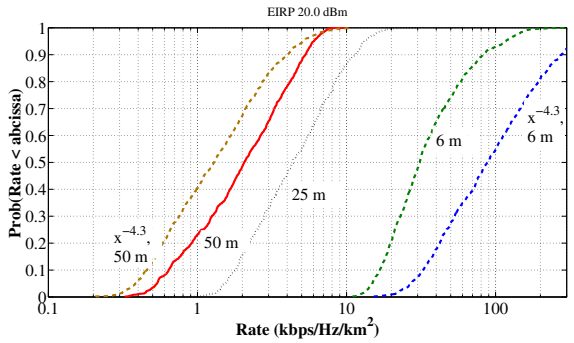

Fig. 7. Area spectral efficiency distribution for different cell separations in the diffuse scattering (indoor) environment. Area rates for $x^{-4.3}$ with 50 m and 6 m cell separation are also shown for reference, appearing as the leftmost and rightmost curves.

its log-normal nature, as well as its standard deviation as a function of range, in good agreement with measurements. It is therefore concluded that diffusion modeling is consistent with observed indoor power variation over the entire observed range. Increasing cell density in such an environment still leads to an increase in wireless network capacity but the gain is materially reduced from what might be anticipated given traditional power-law path loss models.

ACKNOWLEDGMENT

Many thanks to W. M. MacDonald for a helpful discussion on cell-splitting performance.

APPENDIX

It is of interest to determine the extent of log-power variation, quantified by its variance. The integral over $\boldsymbol{\rho}'$ in (17) is recognized as 2D spatial convolution, that may be represented as an inverse Fourier transform of the product of Fourier transforms of its constituent parts, using $dv\left(x',\boldsymbol{\kappa}\right)$ as the random amplitude which is the Fourier transform of $\kappa_{\mathrm{f}}\left(x,\boldsymbol{\rho}\right)$:

$$\psi_{10}=-\int_0^x dx'\iint_{-\infty-\infty}^{\infty\ \infty}\frac{dv\left(x',\boldsymbol{\kappa}\right)}{\left(2\pi\right)^2}\,e^{i\boldsymbol{\kappa}\bullet\boldsymbol{\rho}}\,e^{-\kappa^2\frac{\left(x-x'\right)}{2\bar{\kappa}_{\mathrm{d}}}} \tag{A-1}$$

Here $\boldsymbol{\kappa}$ is the spatial frequency vector, conjugate to the cylindrical coordinate $\boldsymbol{\rho}$, and thus, transverse to x, the line joining the transmitter and receiver. Mean square variation of (A-1) follows as:

$$\left\langle\left|\psi_{10}\right|^2\right\rangle=\int_0^x\int_0^x dx'dx''\iint_{-\infty-\infty}^{\infty\ \infty}\frac{\left\langle dv\left(x',\boldsymbol{\kappa}\right)dv^*\left(x'',\boldsymbol{\kappa}''\right)\right\rangle}{\left(2\pi\right)^4}\times e^{i\left(\boldsymbol{\kappa}-\boldsymbol{\kappa}''\right)\bullet\boldsymbol{\rho}}e^{-\kappa^2\frac{\left(x-x'\right)}{2\bar{\kappa}_{\mathrm{d}}}}e^{-\kappa^2\frac{\left(x-x''\right)}{2\bar{\kappa}_{\mathrm{d}}}} \tag{A-2}$$

The log-power fluctuation (A-1) is an integral over a process $dv\left(x',\boldsymbol{\kappa}\right)$, assumed to be zero-mean and having the spatial correlation represented (appendices A3 and A4 of [24]) in terms of the 2D spectral density $F_{\mathrm{f}}\left(\left|x'-x''\right|,\boldsymbol{\kappa}\right)$ as

$$\left\langle dv\left(x',\boldsymbol{\kappa}\right)dv^*\left(x'',\boldsymbol{\kappa}''\right)\right\rangle=\left(2\pi\right)^2\delta\left(\boldsymbol{\kappa}-\boldsymbol{\kappa}''\right)\times F_{\mathrm{f}}\left(\left|x'-x''\right|,\boldsymbol{\kappa}\right)d\boldsymbol{\kappa}d\boldsymbol{\kappa}'' \tag{A-3}$$

The correlation of (A-1) is assumed to be spatially homogeneous and thus only a function of the difference coordinate $x_{\mathrm{d}}\equiv\left|x'-x''\right|$. In isotropic media the quantity $F_{\mathrm{f}}\left(x_{\mathrm{d}},\boldsymbol{\kappa}\right)$ is related to the 3D spectrum $\Phi_{\mathrm{f}}\left(K\right)$ by

$$\Phi_{\mathrm{f}}\left(\kappa\right)=\int_{-\infty}^{\infty}dx_{\mathrm{d}}F_{\mathrm{f}}\left(x_{\mathrm{d}},\kappa\right) \tag{A-4}$$

Using (A-3),(A-4) in (A-2), the mean square fluctuation of the log-power of the diffuse intensity becomes:

$$\left\langle\left|\psi_{10}\right|^2\right\rangle=\int_0^x dx'\iint_{-\infty-\infty}^{\infty\ \infty}\frac{d\boldsymbol{\kappa}}{\left(2\pi\right)^2}\Phi_{\mathrm{f}}\left(\kappa\right)\,e^{-\kappa^2\frac{\left(x-x'\right)}{\bar{\kappa}_{\mathrm{d}}}} \tag{A-5}$$

The 3D spectrum is defined as the 3D spatial Fourier transform of the 3D correlation function of the fluctuation κ_f and is here assumed to have Gaussian form:

$$\Phi_{\mathrm{f}}\left(\kappa\right)=\left\langle\left|\kappa_{\mathrm{f}}^2\right|\right\rangle\pi^{3/2}l^3e^{-\kappa^2l^2/4} \tag{A-6}$$

where l is the characteristic coherence scale of the (here Gaussian) correlation function of the fluctuating part κ_f of the specific absorption. Physically, regions in the diffuse medium have similar absorption at locations much closer than l and essentially independent absorption at locations separated by much more than l. Substituting (A-6) into (A-5), and integrating out the angular coordinate, we get

$$\left\langle\left|\psi_{10}\right|^2\right\rangle=\left\langle\left|\kappa_{\mathrm{f}}^2\right|\right\rangle\pi^{3/2}l^3\int_0^x dx'\int_0^{\infty}\frac{\kappa d\kappa}{2\pi}e^{-\kappa^2\left(\frac{\left(x-x'\right)}{\bar{\kappa}_{\mathrm{d}}}+l^2/4\right)} \tag{A-7}$$

Following Chapter 18 of Ishimaru [24], the case of spherical wave illumination may be obtained from the plane wave illumination results though the substitution of $\left(x-x'\right)\rightarrow\gamma\left(x-x'\right)$, where $\gamma=x'/x$:

$$\left\langle\left|\psi_{10}\right|^2\right\rangle=\left\langle\left|\kappa_{\mathrm{f}}^2\right|\right\rangle\pi^{3/2}l^3\int_0^x dx'\int_0^{\infty}\frac{\kappa d\kappa}{2\pi}e^{-\kappa^2\left(\frac{x'\left(x-x'\right)}{x\bar{\kappa}_{\mathrm{d}}}+l^2/4\right)} \tag{A-8}$$

Integration over κ yields:

$$\left\langle\left|\psi_{10}\right|^2\right\rangle=\frac{\sqrt{\pi}}{4}\left\langle\left|\kappa_{\mathrm{f}}^2\right|\right\rangle l^3\int_0^x dx'\frac{1}{\frac{x'\left(x-x'\right)}{x\bar{\kappa}_{\mathrm{d}}}+l^2/4} \tag{A-9}$$

Algebraic manipulation yields a standard form:

$$\left\langle\left|\psi_{10}\right|^2\right\rangle=-\frac{\sqrt{\pi}}{4}\left\langle\left|\kappa_{\mathrm{f}}^2\right|\right\rangle l^3x\bar{\kappa}_{\mathrm{d}}\int_0^x\frac{dx'}{x'^2-xx'-x\bar{\kappa}_{\mathrm{d}}l^2/4} \tag{A-10}$$

which may be evaluated in closed form (2.172 in [28]):

$$\left\langle\left|\psi_{10}\right|^2\right\rangle=\frac{\sqrt{\pi}}{4}\left\langle\left|\kappa_{\mathrm{f}}^2\right|\right\rangle\frac{l^3x\bar{\kappa}_{\mathrm{d}}}{\sqrt{-\Delta}}\ln\left(\frac{x+\sqrt{-\Delta}}{x-\sqrt{-\Delta}}\right)^2 \tag{A-11}$$

where $\Delta\equiv-x\bar{\kappa}_{\mathrm{d}}l^2-x^2$ The variance of the log-power is seen to be dependent on range x. Two distinct regions may be identified. In the near zone, $\bar{\kappa}_{\mathrm{d}}l^2>>x$, (A-11) simplifies to

$$\left\langle\left|\psi_{10}\right|^2\right\rangle=\frac{\sqrt{\pi}}{2}\left\langle\left|\kappa_{\mathrm{f}}^2\right|\right\rangle l^3x\bar{\kappa}_{\mathrm{d}}\frac{2x}{-\Delta}\approx\sqrt{\pi}\left\langle\left|\kappa_{\mathrm{f}}^2\right|\right\rangle lx \tag{A-12}$$

At short ranges, the standard deviation of the log-power therefore behaves as

$$\left\langle |\psi_{10}|^2 \right\rangle^{1/2} \approx \sqrt{\pi^{1/2} \left\langle |\kappa_{\rm f}^2| \right\rangle l x} \qquad \text{(A-13)}$$

where it is seen as scaling with range x as $\sqrt{x}$, consistent with 1-D diffusion. In the far range, $\bar{\kappa}_{\rm d} l^2 << x$, (A-11) yields

$$\left\langle |\psi_{10}|^2 \right\rangle^{1/2} \approx \sqrt{\frac{\pi^{1/2}}{2} \left\langle |\kappa_{\rm f}^2| \right\rangle l^3 \bar{\kappa}_{\rm d} \ln \left| \frac{4x}{\bar{\kappa}_{\rm d} l^2} \right|} \qquad \text{(A-14)}$$

REFERENCES

[1] R. A. Valenzuela, "A ray tracing approach to predicting indoor wireless transmission," *1993 IEEE Vehicular Technology Conference*.

[2] S. J. Fortune, D. M. Gay, B. W. Kernighan, O. Landron, R. A. Valenzuela, and M. H. Wright, "WISE design of indoor wireless systems," *IEEE Computational Science and Engineering*, vol. 2, no. 1, pp. 58–68, 1995.

[3] D. J. Cichon, T. Zwick, and J. Lahteenmaki, "Ray optical indoor modeling in multi-floored buildings: simulations and measurements," *1995 Ant. and Prop. Soc. Int. Symp.*

[4] M. Porebska, T. Kayser, and W. Wiesbeck, "Verification of a hybrid ray-tracing/FDTD model for indoor ultra-wideband channels," *2007 European Conf. on Wireless Technologies.*

[5] J. Jemai, R. Piesiewicz, and T. Kurner, "Calibration of an indoor radio propagation prediction model at 2.4 GHz by measurements of the IEEE 802.11b preamble," *2005 Vehicular Technology Conference*.

[6] Y. Okumura, E. Ohmori, T. Kawano, and K. Fukuda, "Field strength hand its variability in VHF and UHF land-mobile radio service," *Rev. Elect. Com. Lab*., vol. 16, pp. 825–873, 1968.

[7] M. Hata, "Empirical formula for propagation loss in land mobile radio services," *IEEE Trans. Veh. Technol.*, vol. 29, no. 3, pp. 317–325, Aug. 1980.

[8] S. S. Ghassemzadeh, L. J. Greenstein, A. Kavcic, T. Sveinsson, and V. Tarokh, "UWB indoor path loss model for residential and commercial buildings," *2003 IEEE Vehicular Technology Conference*.

[9] S. S. Ghassemzadeh and V. Tarokh, "UWB path loss characterization in residential environments," *2003 IEEE Radio Frequency Integrated Circuits Symposium*.

[10] COST Action 231, "Digital mobile radio towards future generation systems, final report," technical report, European Communities, EUR 18957, 1999.

[11] J. Walfisch and H. L. Bertoni, "A theoretical model of UHF propagation in urban environments," *IEEE Trans. Antennas Propag*., vol. 36, no. 12, pp. 1788–1796, Dec. 1988.

[12] D. Chizhik and J. Ling, "Propagation over clutter: physical stochastic model," *IEEE Trans. Antennas Propag.*, vol. 56, no. 4, pp. 1071–1077, Apr. 2008.

[13] W. Honcharenko, H. L. Bertoni, J. L. Dailing, J. Qian, and H. D. Yee, "Mechanisms governing UHF propagation on single floors in modern office buildings," *IEEE Trans. Veh. Technol.*, vol. 41, pp. 496–504, Nov. 1992.

[14] D. M. J. Devasirvatham, C. Banerjee, R. R. Murray, and D. A. Rappaport, "Four-frequency radiowave propagation measurements of the indoor environment in a large metropolitan commercial building," *1991 Global Telecommunications Conference*.

[15] J. Medbo and J.-E. Berg, "Simple and accurate path loss modeling at 5 GHz in indoor environments with corridors," *2000 IEEE Vehicular Tech. Conf. – Fall*.

[16] D. M. J. Devasirvatham, C. Banerjee, M. J. Krain, and D. A. Rappaport, "Multi-frequency radiowave propagation measurements in the portable radio environment," *1990 IEEE International Conf. on Commun.*

[17] J. M. Keenan and A. J. Motley, "Radio coverage in buildings," *British Telecom Technol. J.*, vol. 8, no. 1, Jan. 1990.

[18] D. Ullmo and H. U. Baranger, "Wireless propagation in buildings: a statistical scattering approach," *IEEE Trans. Veh. Technol.*, vol. 48, no. 3, pp. 947–955, May 1999.

[19] R. Janaswamy, "An indoor path loss model at 60 GHz based on transport theory," *IEEE Antennas Wireless Propag. Lett.*, vol. 5, no. 1, pp. 58–60, Dec. 2006.

[20] M. Franceschetti, J. Bruck, and L. J. Schulman, "A random walk model of wave propagation," *IEEE Trans. Antennas Propag.*, vol. 52, bo. 5, pp. 1304–1317, May 2004.

[21] W. Honcharenko, H. L. Bertoni, and J. Dailing, "Mechanisms governing propagation between different floors in buildings," *IEEE Trans. Antennas Propag.*, vol. 41, no. 6, pp. 787–790, June 1993.

[22] N. Yarkony and N. Blaunstein, "Prediction of propagation characteristics in indoor radio communication environments," *2007 European Conf. on Antennas and Propagation*.

[23] J. Baker-Jarvis, M. D. Janezic, R. F. Riddle, R. T. Johnk, P. Kabos, C. Holloway, R. G. Geyer, and C. A. Grosvenor, "Measuring the permittivity and permeability of lossy materials: solids, liquids, metals, building materials, and negative-index materials," National Institute of Science and Technology, NIST Technical Note 1536, 2005.

[24] A. Ishimaru, *Wave Propagation and Scattering in Random Media*. IEEE Press Series on Electromagnetic Wave Theory, 1997.

[25] S. M. Rytov, Yu. A. Kravtsov, V. I. Tatarskii, *Principles of Statistical Radiophysics: Wave Propagation Through Random Media*. Springer-Verlag, 1989.

[26] R. A. Valenzuela, O. Landron, and D. L. Jacobs, "Estimating local mean signal strength of indoor multipath propagation," *IEEE Trans. Veh. Technol.*, vol. 46, no. 1, pp. 203–212, Feb 1997.

[27] J. Ling and D. Chizhik, "Capacity scaling of indoor pico-cellular networks via reuse," *IEEE Commun. Lett.*, vol. 16, no. 2, pp. 231-233, Feb. 2012.

[28] I. S. Gradshteyn and I. M. Ryzhik, *Table of Integrals, Series, and Products*, 4th edition. Academic Press, 1965.

Dmitry Chizhik received a Ph.D. in Electrophysics at the Polytechnic University, Brooklyn, NY. His thesis work has been in ultrasonics and non-destructive evaluation. He joined the Naval Undersea Warfare Center, New London, CT where he did research in scattering from ocean floor, geoacoustic modeling of porous media and shallow water acoustic propagation. In 1996 he has joined Bell Laboratories, working on radio propagation modeling and measurements, using deterministic and statistical techniques. He has worked on measurement, modeling and channel estimation of MIMO channels. The results are used both for determination of channel-imposed bounds on channel capacity, system performance, as well as for optimal antenna array design. His recent work has included system and link simulations of satellite and femto cell radio communications that included all aspects of the physical layer. His research interests are in acoustic and electromagnetic wave propagation, signal processing,communications, radar, sonar, medical imaging.

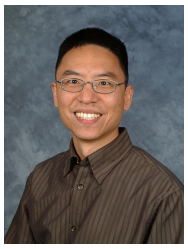

Jonathan Ling received the B.Sc degree in electrical engineering from Rutgers, Piscataway, NJ, and M.Sc. in computer science and PhD in electrical engineering both from Stevens Institute, Hoboken, NJ. He joined the Wireless Communications Research Department of Bell Laboratories, Holmdel, NJ in 1994. He has conducted MIMO radio propagation measurements and modeling, and helped develop the WiSE ray-tracing tool. His research interests are media access, wireless systems, channel modeling, and signal processing.

Reinaldo A. Valenzuela B.Sc. University of Chile, Ph.D. Imperial College. IEEE Fellow. 2010 IEEE Eric E. Sumner Award. Director, Wireless Communications Research Department, Distinguished Member of Technical Staff, Bell Laboratories. Engaged in MIMO/space time systems achieving high capacities using transmit and receive antenna arrays. He has published over 130 papers and 12 patents. He has over 15000 Google Scholar citations and is a 'Highly Cited Author' In Thomson ISI and a Fulbright Senior Specialist.